University of
Strathclyde
Glasgow

Strathprints Institutional Repository

http://strathprints.strath.ac.uk/

A Theoretical Analysis of a Piezoelectric Ultrasound Device with an Active Matching Layer

Anthony J. Mulholland[†][*], Richard L. O'Leary[‡],

Nishal Ramadas[‡], Agnes Parr[‡], Alexandre Troge[§],

Richard A. Pethrick[§], and Gordon Hayward[‡]

[†] Department of Mathematics, University of Strathclyde,

Glasgow, UK G1 1XH

[‡] The Centre for Ultrasonic Engineering,

Department of Electronic and Electrical Engineering,

University of Strathclyde, Glasgow, UK G1 1XW

[§] Department of Pure and Applied Chemistry,

University of Strathclyde, Glasgow, U.K. G1 1XL

August 9, 2007

[*]Address for correspondence: Department of Mathematics, University of Strathclyde, Livingstone Tower, 26 Richmond Street, Glasgow G1 1XH, U.K., Tel: ++44 (0)141 548 2971, Fax: ++44 (0)141 548 3345, email: ajm@maths.strath.ac.uk

1

Abstract

This paper investigates the use of magnetically active materials in the matching layer of a piezoelectric transducer. This then allows the performance of the device to be dynamically altered by applying an external field. The effect that this new matching layer has on the performance of a typical device is theoretically investigated here. It transpires that the additional flexibility of an active matching layer can be used to maintain the efficiency of the device as the external load is varied.

Keywords: MAGNETORHEOLOGICAL, ULTRASONIC TRANSDUCER, MATCHING LAYER, MODELLING

PACS Code: 43.35.+d

1   Introduction

The transmission and detection of ultrasonic energy forms the basis for a large number of modern instrumentation and measurement systems. Applications include biomedical therapy and diagnosis, underwater sonar, non-destructive testing, structural condition monitoring, industrial processing and analysis, and materials characterisation. The requirement for efficient generation and detection over a desired frequency band is paramount and very often the limiting component of the entire system relates to the front end transducer design [1]. These transducers comprise of an active piezoelectric layer sandwiched between a backing material for damping and bandwidth control and some form of matching layer for interfacing to the mechanical load medium. Sensitivity and bandwidth depend on the efficiency of the active material, the quality of matching to the load and the degree of damping. The operating frequency is governed by the active piezoelectric layer and to a slightly lesser extent, by the properties of the front face matching layer. Since it is a resonant system, sensitivity and bandwidth also tend to be mutually exclusive, with the highest sensitivity being achieved under narrowband, low loss, resonant conditions. This is often in direct conflict with many of the new application requirements, such as harmonic imaging, where detection of the upper, even harmonics is required and high resolution, high frequency sonar, where pulse compression methods are needed to achieve an adequate signal to noise ratio. The standard front face matching, by means of a quarter wavelength layer, is effective only over a relatively narrow frequency range. This paper investigates the possibility of using magnetically active materials in the matching layer so that, by applying an external field, the resonant behaviour of the device can be dynamically altered. There has been considerable interest in recent years in the area of magnetorheological fluid [2]. Application of an external magnetic field rapidly induces alignment of conducting particles suspended in a viscous fluid. This in turn changes the mechanical properties of the material. For thickness mode transducers, the dynamics can be approximately described

3

by a one-dimensional model. By coupling the piezoelectric constitutive equations with the one-dimensional wave equation for the mechanical displacement, the linear systems model (LSM) can be derived [3]. In a series of papers, the dependency of both the reception and transmission characteristics of transducers with passive (i.e. non-active) matching layers has been investigated [4, 5, 6].

In the next section the key equations in the LSM model are presented and the resulting multilayer matrix formulation described. In Section 3 a model of the magnetorheological matching layer is presented. Section 4 then investigates the effect that this new matching layer has on the performance of a typical device. It is found that the additional flexibility of an active matching layer can be used to maintain the efficiency of the device as the external load is varied.

2   Linear Systems Modelling

Composite transducers, consisting of a low impedance passive phase combined with the piezoelectric ceramic, do lower the effective mechanical impedance, thereby improving front face matching and bandwidth. Composite transducers are typically manufactured by slicing the piezoelectric ceramic into a bristle block of vertical pillars and then filling the inter-pillar space with a passive polymer. Since the ceramic has a connectivity in only one direction whilst the polymer has connectivity in all three directions, this topology is described as 1-3 (see Figure 1).

In order to utilise the LSM the effective properties of the 1-3 composite transducer must be derived [7]. The piezoelectric constitutive equations can be described, when the electric field and the strain are chosen as independent coordinates, as [8]

$$T_i = c_{ij}S_j - e_{ij}E_j, \tag{1}$$

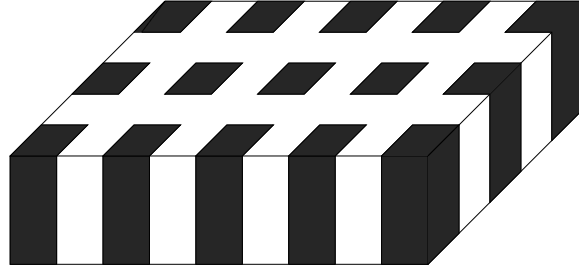$$D_i = e_{ij}S_j + \epsilon_{ij}E_j \tag{2}$$

4

Figure 1: Illustration of a 1-3 composite transducer where the ceramic is black and the polymer is white.

for $i, j = 1, 2, 3$, where T_i is the stress tensor, S_i is the strain tensor, c_{ij} are the elastic stiffnesses, D_i is the electric displacement vector, $e_{ij} = h_{im}\epsilon_{mj}$ are the piezoelectric stress coefficients, ϵ_{ij} are the permittivity coefficients and E_j is the external electric field vector [10, 8] (in the passive polymer phase $e_{ij} = 0$). A well known model exists to obtain the averaged constitutive relations of a 1-3 composite assuming a set of constraints that, being strong, are good approximations of the real physical situation [7]. These conditions are (i) the electric field and the strain are functions of z only, where z is directed along the pillar length (the vertical direction in Figure 1), (ii) the transducer is a large thin plate, (iii) the ceramic and polymer move together in the z direction, (iv) the electric field is the same in both phases, (v) the lateral stresses are equal in both phases and (vi) the lateral periodicity is sufficiently fine that the effective total stress $\bar{T}_3$ and electric displacement $\bar{D}_3$ can be approximated by volume averaging [7]. The effective constitutive equations are then

$$\bar{T}_3 = \bar{c}_{33}^D \bar{S}_3 - \bar{h}_{33}\bar{D}_3 \tag{3}$$

$$\bar{E}_3 = -\bar{h}_{33}\bar{S}_3 + \bar{\beta}_{33}\bar{D}_3 \tag{4}$$

where $c_{33}^D = \bar{c}_{33} + (\bar{e}_{33})^2/\bar{\epsilon}_{33}$, the piezoelectric constant is $\bar{h}_{33} = \bar{e}_{33}/\bar{\epsilon}_{33}$ and $\bar{\beta}_{33} = 1/\bar{\epsilon}_{33}$. The one-dimensional wave equation for the mechanical displacement $u(x, t)$ is

$$\bar{\rho}\frac{\partial^2 u(x, t)}{\partial t^2} = \bar{c}_{33}^D \frac{\partial^2 u(x, t)}{\partial x^2} \tag{5}$$

5

where $\bar{\rho}$ is the volume averaged density, and the boundary conditions of continuity of displacement and force into the adjacent media apply. For a complete transducer system composed of an active piezocomposite resonator, a backing material at the rear piezocomposite mechanical port (subscript B), a resonant matching layer at the front mechanical port (subscript M) and a real load as the propagating medium, the equations for the mechanical displacement, the force and the voltage at each transducer interface can be derived by transforming the above equations into the Laplace domain and assuming that (i) there is no initial displacement or velocity, (ii) there is no free charge inside the transducer and so Gauss's Law can be applied, and (iii) the transducer is placed in parallel with a load impedance Z_E and the combination is placed in series with a load Z_0 as shown in Figure 2. The equations are as follows
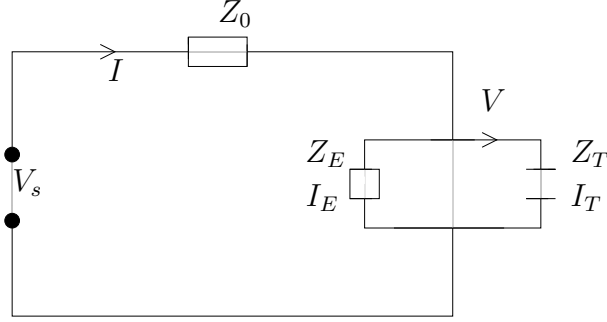

Figure 2: Schematic of the transducer circuit.

$$u_i = A_i e^{-\frac{sx}{v_i}} + B_i e^{\frac{sx}{v_i}}, \tag{6}$$

$$F_i = sZ_{c_i}\left(-A_i e^{-\frac{sx}{v_i}} + B_i e^{\frac{sx}{v_i}}\right) + \frac{h_i \bar{V}_i}{sb} - \frac{h_i \bar{V}_s}{sZ_0}, \tag{7}$$

$$\bar{V}_T = -Uh_{33}\left(A_T(e^{-st_T} - 1) + B_T(e^{st_T} - 1)\right) + \frac{UV_s}{sZ_0 C_{0_T}}, \tag{8}$$

where $Z_{c_i} = \rho_i v_i A_r$ is the acoustic impedance of layer i, ρ_i is the density of layer i, A_r is the cross-sectional area, v_i is the velocity of a longitudinal wave in layer i, s is the Laplace variable, V_i is the voltage in layer i, V_s is the circuit driving voltage, $C_{0_T} = A_r \bar{\epsilon}_{33}/L_T$ is the

clamped capacitance of the piezoelectric layer, L_i is the thickness of layer i, t_i is the transit time of a longitudinal wave in layer i, $U = sC_{0_T}b/(1 + sC_{0_T}b)$, and $b = Z_E Z_0/(Z_E + Z_0)$. At each layer interface, continuity of displacement and force is imposed. In the backing layer it is assumed that the incoming wave is damped as it travels to the left and hence there is no reflected wave travelling to the right in this region, that is $A_B = 0$. In a similar way, by assuming that the mechanical load is infinite in extent, we obtain $B_L = 0$. In each layer a local coordinate system is used to simplify the algebra and the resulting set of algebraic equations can be expressed in matrix form as $\Xi\, \underline{\nu} = \underline{\zeta}$ where

$$\Xi = \begin{bmatrix} 1 & -1 & -1 & 0 & 0 & 0 & 0 \\ sZ_B & sZ_T & -sZ_T & 0 & 0 & 0 & h_{33}U(e^{-st_T}-1) \\ 0 & e^{-st_T} & e^{st_T} & -1 & -1 & 0 & h_{33}U(e^{st_T}-1) \\ 0 & -sZ_T e^{-st_T} & sZ_T e^{st_T} & sZ_M & -sZ_M & 0 & 0 \\ 0 & 0 & 0 & e^{-st_M} & e^{st_M} & -1 & 0 \\ 0 & 0 & 0 & -sZ_M e^{-st_M} & sZ_M e^{st_M} & sZ_L & 0 \\ 0 & -h_{33}/(sb) & h_{33}/(sb) & 0 & 0 & 0 & 1 \end{bmatrix},$$

$$\underline{\nu} = \begin{bmatrix} B_B & A_T & B_T & A_M & B_M & A_L & V_T \end{bmatrix}^T,$$

and

$$\underline{\zeta} = \begin{bmatrix} 0 & -h_{33}V_s/(sZ_0) & 0 & h_{33}V_s/(sZ_0) & 0 & 0 & UV_s/(sZ_0C_{0_T}) \end{bmatrix}^T.$$

By solving this system for $\underline{\nu}$ the electrical and mechanical behaviour of the transducer can be analysed. In particular the electrical impedance of the device is given by

$$Z_T = \frac{V_T b}{aV_s - V_T} \tag{9}$$

where $a = Z_E/(Z_0 + Z_E)$, and the transmission sensitivity is given by

$$\Phi(\omega) = \frac{F_L(0)}{V_s} = \frac{-sZ_T A_L}{V_s}. \tag{10}$$

7

The transmission voltage response (TVR), in decibels, is then given by $\text{TVR} = 20 \log_{10}(\Phi(\omega))$. In the next section a potential matching layer material is discussed whose properties can be dynamically altered by the use of a magnetic field. The effect that this has on the electrical and mechanical behaviour of a typical device is then presented.

3 Magnetorheological Matching Layer

Recent work on a the propagation of elastic waves in magnetorheological fluids has shown that a large change in the longitudinal wave velocity (around fifty percent) can be achieved by the application of a magnetic field [2]. The material consists of hard, spherical particles randomly suspended in a viscous carrier fluid. The application of the external field aligns the particles into columnar structures by forming magnetic dipole-dipole interactions between them. This stiffens the material and increases the longitudinal wave velocity in the direction parallel to this alignment. The resonant behaviour of the transducers described in the previous section depends on the mechanical coupling between the three layers (backing, piezoelectric and matching). Therefore, by using a matching layer that can change its mechanical properties the electrical and mechanical behaviour of the entire device is affected. To incorporate this effect into the LSM, a model of wave propagation in a suspension of particles in a fluid [9] is supplemented by an empirically derived expression for a magnetic field enhancement of the effective particle volume fraction [2].

Using a coupled-phase model the effective velocity in the matching layer is given by $\bar{v}_M = \Re(\omega/k)$ where [9]

$$k = \sqrt{\frac{\omega^2((1-\varphi)\beta_f + \varphi\beta_p)\rho_f(\rho_p(1 - \varphi + \varphi\psi) + \rho_f\psi(1-\varphi))}{\rho_p(1-\varphi)^2 + \rho_f(\psi + \varphi(1-\varphi))}}, \tag{11}$$

$$\psi = \frac{1}{2}(\frac{1+2\varphi}{1-\varphi}) + \frac{9\delta}{4p} + i\frac{9}{4}(\frac{\delta}{p} + \frac{\delta^2}{p^2}), \tag{12}$$

$\delta = \sqrt{2\eta/(\omega\rho_f)}$, $\eta = \eta_f(1 + 2.5\varphi + 7.3\varphi^2)$, the compressibility of the particles (and the fluid) is $\beta_p = 1/(\rho_p v_p^2)$ (and $\beta_f = 1/(\rho_f v_f^2)$), η_f is the fluid viscosity, φ is the volume fraction of the

particles of diameter p, $v_{p/f}$ is the longitudinal wave velocity in the particle/fluid, $\rho_{p/f}$ is the density of the particles/fluid, ω is the angular driving frequency and k is the wavenumber. The presence of the magnetic field aligns the particles into columnar structures and the mechanical energy is then conveyed through the resulting fluid channels that contain a far smaller volume fraction of particles (φ_{sat}). This effect is captured by the model by using the magnetic field strength H to enhance the particle volume fraction via the empirical relationship [2]

$$\bar{\varphi} = (\varphi - \varphi_{sat})e^{-cH} + \varphi_{sat} \tag{13}$$

where $\varphi_{sat} = 0.052$ is the effective volume fraction of the particles for very high magnetic field amplitudes, and $c = 0.0091$. As the volume fraction of particles increases from zero the effective longitudinal wave velocity of the material decreases from the pure fluid's value down to a minimum at around $\varphi = 0.4$ and then it rises monotonically until it attains the particle's value at $\varphi = 1$. At typical particle volume fractions of around $\varphi = 0.3$ the addition of the magnetic field will give rise to a smaller effective particle volume fraction ($\bar{\varphi}$) and hence the longitudinal velocity will increase.

In the next section, numerical results from the combined models of this section and the previous one are shown. It transpires that the matrix Ξ is ill-conditioned due to the large variations in the magnitudes of the various parameters (for example 20 orders of magnitude can exist between elastic moduli and the permittivities). To alleviate this problem the matrix entries are balanced by scaling the parameters of the model (see Table 1). Each of the parameters is made, as close as is feasible, $O(1)$ by a judicious choice of the scalings α, β, γ and φ in terms of the fundamental units of length ($\bar{L} = \beta L$), mass ($\bar{M} = \alpha M$), time ($\bar{T} = \gamma T$) and charge ($\bar{C} = \phi C$). This is done by scaling the layer thickness L by specifying β, scaling the density ρ by specifying α, scaling the piezoelectric stress tensor e_{ijk} by specifying ϕ, scaling the elasticity tensor c_{ijkl} by specifying γ and this results in an appropriate scaling for the permittivity tensor ϵ_{ij}. The electrical and mechanical units are

related to each other via energy considerations.

Parameter	Typical Size	Units	Dimensions	Scaling	Typical Scaling
c_{ijkl}	10^{11}	Nm^{-2}	$ML^{-1}T^{-2}$	$\alpha\beta^{-1}\gamma^{-2}$	10^{-11}
ϵ_{ij}	10^{-9}	Fm^{-1}	$M^{-1}L^{-3}T^{2}C^{2}$	$\phi^{2}\alpha^{-1}\gamma^{2}\beta^{-3}$	10^{9}
e_{ijk}	10	Cm^{-2}	CL^{-2}	$\phi\beta^{-2}$	10^{-1}
ρ	10^{3}	kgm^{-3}	ML^{-3}	$\alpha\beta^{-3}$	10^{-3}
L	10^{-3}	m	L	β	10^{4}
A_r	10^{-4}	m^{2}	L^{2}	β^{2}	10^{8}
V_T	10	V	$ML^{2}T^{-2}C^{-1}$	$\alpha\beta^{2}\gamma^{-2}\phi^{-1}$	10^{-6}
ω	10^{6}	rad s^{-1}	T^{-1}	γ^{-1}	10^{-8}
Z_E	10^{2}	Ω	$ML^{2}T^{-1}C^{-2}$	$\alpha\beta^{2}\gamma^{-1}\phi^{-2}$	10^{-5}
η	10	Nsm^{-2}	$ML^{-1}T^{-1}$	$\alpha\beta^{-1}\gamma^{-1}$	10^{-3}
Z_c^s	10^{6}	Rayls	$ML^{-2}T^{-1}$	$\alpha\beta^{-2}\gamma^{-1}$	10^{-7}
C_{0_T}	10^{-9}	Farads	$M^{-1}L^{-2}T^{2}C^{2}$	$\alpha^{-1}\beta^{-2}\gamma^{2}\phi^{2}$	10^{13}
h_{33}	10^{9}	Vm^{-1}	$MLT^{-2}C^{-1}$	$\alpha\beta\gamma^{-2}\phi^{-1}$	10^{-10}
F	10^{4}	N	MLT^{-2}	$\alpha\beta\gamma^{-2}$	10^{-3}
v_i	10^{3}	ms^{-1}	LT^{-1}	$\beta\gamma^{-1}$	10^{-4}
$\Phi(\omega)$	10^{3}	N/V	$L^{-1}C$	$\beta^{-1}\phi$	10^{3}

Table 1: Dimensions and scaling parameters ($\beta = 10^4$, $\gamma = 10^8$, $\phi = 10^7$ and $\alpha = 10^9$).

4   Results

The results in this section pertain to a transducer that has a 1-3 piezocomposite resonator with a PZ29 piezoceramic [12] (see Table 2) and a HY1300/CY1301 polymer [13] (see Table 3) giving rise to the effective properties detailed in Table 4. The device dimensions,

the load and backing material parameters and the electrical circuit details are given in Table 5, and the active matching layer parameters are given in Table 6.

Parameter	Units	Value
c_{11}	Nm^{-2}	13.4×10^{10}
c_{12}	Nm^{-2}	8.97×10^{10}
c_{13}	Nm^{-2}	8.57×10^{10}
c_{33}	Nm^{-2}	10.91×10^{10}
ϵ_{33}	$\mathrm{F\ m}^{-1}$	1.08×10^{-8}
ρ	$\mathrm{kg\ m}^{-3}$	7.46×10^{3}
e_{33}	$\mathrm{C\ m}^{-2}$	21.2
e_{31}	$\mathrm{C\ m}^{-2}$	-5.06

Table 2: Physical properties of the ceramic phase PZ29 [12].

Parameter	Units	Value
c_{11}	$\mathrm{kg\ m}^{-1}\mathrm{s}^{-2}$	7.33×10^{9}
c_{12}	$\mathrm{kg\ m}^{-1}\mathrm{s}^{-2}$	4.22×10^{9}
v_s	$\mathrm{m\ s}^{-1}$	1.17×10^{3}
v_L	$\mathrm{m\ s}^{-1}$	2.54×10^{3}
ρ	$\mathrm{kg\ m}^{-3}$	1.15×10^{3}
ϵ	-	3.54×10^{-11}

Table 3: Physical properties of the polymer phase HY1300/CY1301 Hardset [11].

The backing layer impedance is given by $Z_B = \rho_B v_B A_r$ where $v_B = (1 - \nu_B)/((1 + \nu_B)(1 - 2\nu_B))Y_B/\rho_B$, ν_B is its Poisson ratio, Y_B its Young's modulus and ρ_B its density. There are several metrics which are used to describe the transmission voltage response

Parameter	Units	Value
c_{33}^e	N m^{-2}	3.10×10^{10}
h_{33}	V m^{-1}	2.23×10^9
ϵ_{33}^e	F m^{-1}	5.75×10^{-9}
v_T	m s^{-1}	3668
ρ_T	kg m^{-3}	4.43×10^3
$Z_{c_T}^s$	Rayls	16.20×10^6

Table 4: Effective properties of the ceramic and hardset polymer phase using [7], with a ceramic volume fraction of 0.52.

Parameter	Units	Value
L_T	m	1.9×10^{-3}
L_M	m	0.51×10^{-3}
Y_B	N m^{-2}	6×10^7
ρ_B	kg m^{-3}	1.2×10^3
ν_B	-	0.4
Z_B	Rayls	2×10^6
A_r	m^2	1×10^{-4}
Z_0	Ω	50
Z_E	Ω	1×10^7
V_s	V	1
Z_L	Rayls	1.5×10^6

Table 5: Dimensions of the transducer, backing layer material properties, and electrical circuit impedances.

Parameter	Units	Value
p	μm	12
ρ_f	kg m^{-3}	1.26×10^3
ρ_p	kg m^{-3}	7.86×10^3
η_f	N s m^{-2}	1.5
v_p	m s^{-1}	5.18×10^3
v_f	m s^{-1}	1.89×10^3

Table 6: Properties of the fluid (f) phase (glycerine) and the solid particle phase (p) (iron) [2].

(TVR) including the ringdown time (R), which gives the duration of the response of the transducer to an impulse voltage. The time domain response is calculated from an Inverse Fast Fourier Transform of the Transmission Sensitivity frequency spectrum ($\Phi(\omega)$) generated using equation (10). Due to the oscillations in the resulting signal an integration is performed to smooth out the change in the ringdown as a function of the system parameters. Of particular interest here is the change in ringdown time as the magnetic field is changed and as the volume fraction of particles is changed. Therefore the ringdown time is calculated here using

$$R = \left\{ \tau : \frac{\int_0^\tau \hat{\Phi}(t)dt}{\int_0^\infty \hat{\Phi}(t)dt} = 0.9 \right\}. \tag{14}$$

A measure that is used in the frequency domain is the 3dB bandwidth (BW_3)of the TVR which gives a measure of the range of frequency over which the device can operate at a reasonable level. It is worth noting that bimodal spectra can introduce discontinuities in the bandwidth when viewed as a function of the system parameters. These discontinuities arise at the parameter values where the maximum amplitude (TVR(f_{max})) shifts from one of the peaks to the other. This can be partially alleviated by calculating the bandwidth

13

using

$$BW_3 = (f_r - f_l)/((f_r + f_l)/2) \times 100 \tag{15}$$

where $f_r = min\{f : f > f_{max}$ and $\text{TVR}(f) = \text{TVR}(f_{max}) - 3\}$ and $f_l = max\{f : f < f_{max}$ and $\text{TVR}(f) = \text{TVR}(f_{max}) - 3\}$. The Gain Bandwidth Product (GBP) is then given by $\text{GBP} = \text{TVR}(f_{max}) \times BW_3$. To calculate the optimum thickness of the matching layer, in terms of the 3dB bandwidth, the volume fraction of particles (φ) in the matching layer was found such that $Z_M(\varphi) = \sqrt{Z_L Z_T}$. A plot of the conductance of this device, with an air load $(Z_L = 410)$, as a function of frequency was then constructed and the thickness of the matching layer (L_M) was adjusted until the amplitudes of the two conductance peaks were identical.
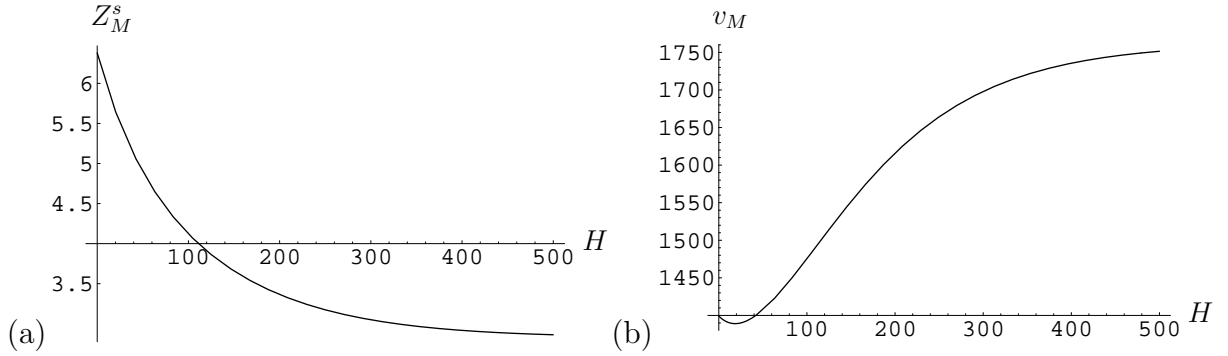

Figure 3: (a) The specific mechanical impedance of the matching layer $(Z_M^s(\text{MRayls}))$ and (b) the longitudinal wave velocity in the matching layer $(v_M \ (\text{ms}^{-1}))$, versus the magnetic field strength $(H \ (\text{Gauss}))$.

In Figure 3(a) the specific mechanical impedance (Z_M^s) of the matching layer is shown as a function of the magnetic field strength H. The volume fraction of spherical iron particles is fixed at $\varphi = 0.5$. In a standard device the optimal mechanical impedance of the matching layer can be approximately given by the geometric mean of the mechanical impedances of the two adjacent layers (see Tables 5 and 4). For the materials used here this value is 4.9 MRayls and this corresponds to a magnetic field strength of approximately $H = 50$ Gauss.
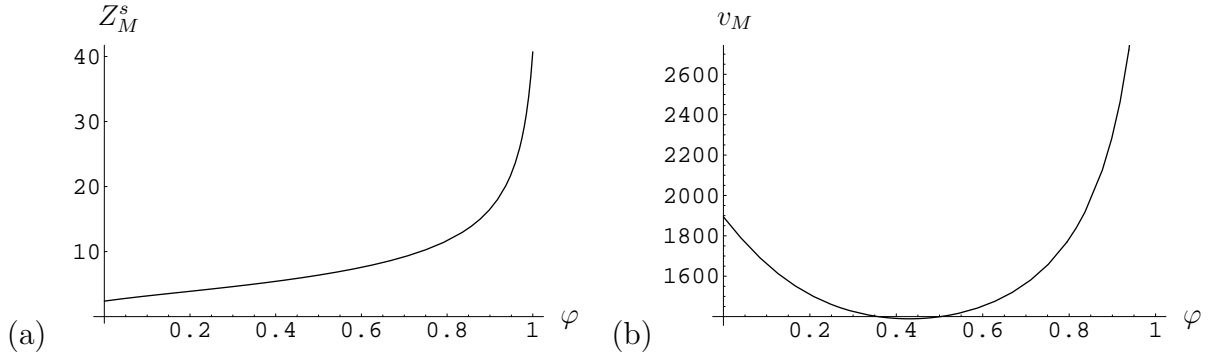
14

Figure 4: (a) The specific mechanical impedance of the matching layer (Z_M^s(MRayls)) and (b) the longitudinal wave velocity in the matching layer (v_M (ms^{-1})), versus the volume fraction of particles in the matching layer (φ).

This material will therefore provide an excellent coupling between the piezocomposite and the mechanical load. As the magnetic field strength increases the mechanical impedance decreases. This is due to the particles aligning and allowing the longitudinal wave to propagate unhindered in the relatively low mechanical impedance fluid. As H increases the model lowers the effective volume fraction of particles according to equation (13), and the optimal effective volume fraction is roughly $\bar{\varphi} = 0.3$. In Figure 3(b) the corresponding longitudinal wave velocity is seen to increase, after an initial minimum, as the magnetic field strength is increased. However the effective density decreases at a faster rate and the net effect is a reduction in the mechanical impedance. In equation (12) this lowering of the effective volume fraction of particles ($\bar{\varphi}$) decreases the viscosity η, which decreases δ and this results in the magnitude of ψ decreasing. The effect that this has on the wave number k in equation (11) is complicated but after an initial phase it decreases monotonically leading to the observed increase in phase velocity v_M. This velocity remains below that of the fluid v_f and for very large H the velocity will asymptote to this value (see Table 6). In Figure 4(a) the specific mechanical impedance is plotted as a function of the volume fraction of particles φ in the active matching layer. Throughout the magnetic field is absent and the value of

15

the mechanical impedance at $\varphi = 0.5$ corresponds to the initial value in Figure 3(a). It can be seen that the optimal mechanical impedance value of 4.9 MRayls corresponds to a lower particle volume fraction of around $\varphi = 0.3$. As the particles are not aligned here then by increasing the volume fraction of the relatively high mechanical impedance iron particles the overall mechanical impedance for the matching layer increases. Although the velocity profile in Figure 4(b) has a pronounced minimum the density of the iron particles is far greater than that of the supporting fluid and dominates the resulting mechanical impedance calculation (see Table 6). As φ increases the effective viscosity η increases, leading to increases in δ and ψ in equation (12). The complex dependency of the wave number k on φ in equation (11) leads to the quadratic shaped profile for the effective velocity shown in Figure 4(b). It can be seen that this curve links the fluid velocity (v_f) at $\varphi = 0$ to the particle velocity (v_p) at $(\varphi = 1)$ (see Table 6). At intermediate volume fractions the random orientation of the iron particles creates a tortuous path for the wave energy to traverse leading to a longer transit time than that in either of the pure materials.
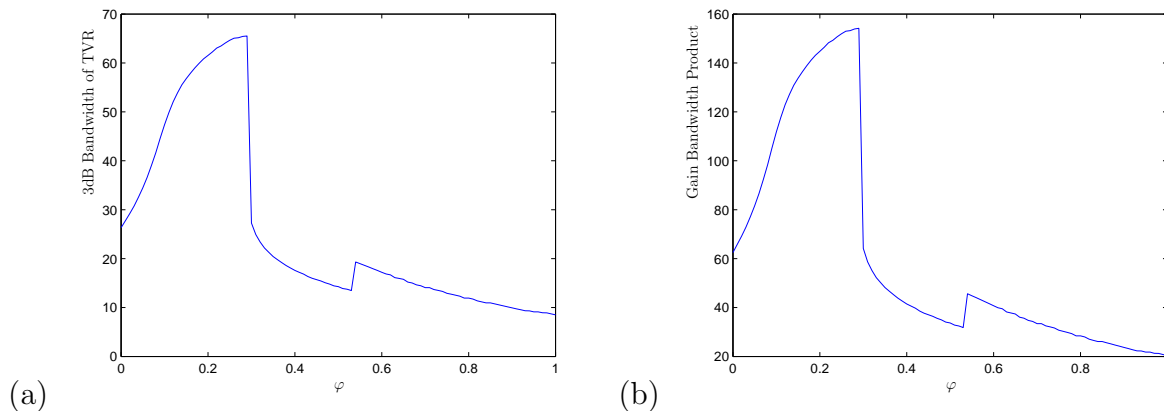

Figure 5: (a) The 3dB bandwidth of the Transmission Voltage Response (TVR) and (b) the Gain Bandwidth Product, versus the volume fraction of particles in the matching layer (φ).

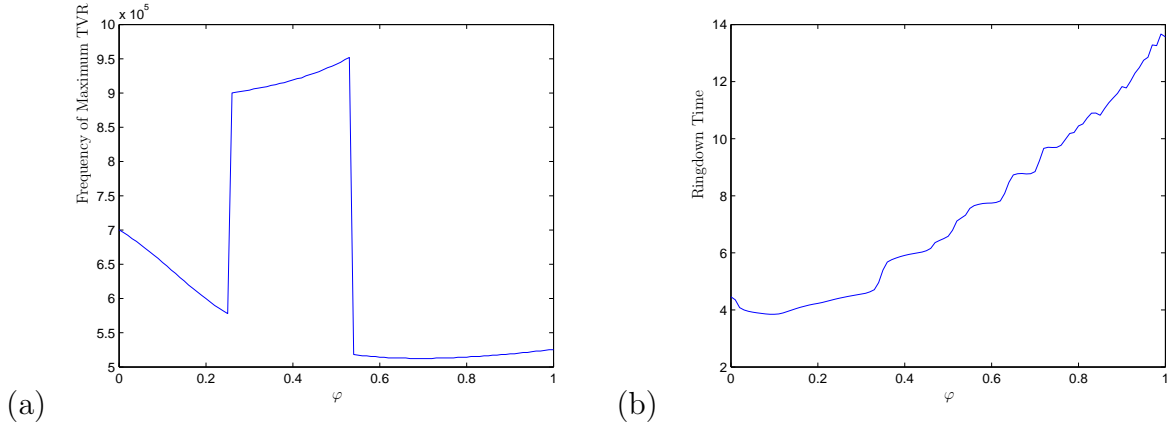In the set of figures that now follow, the LSM model is used to calculate the various

Figure 6: (a) The frequency (Hz) of the peak Transmission Voltage Response and (b) the ringdown time (μs), versus the volume fraction of particles in the matching layer (φ).
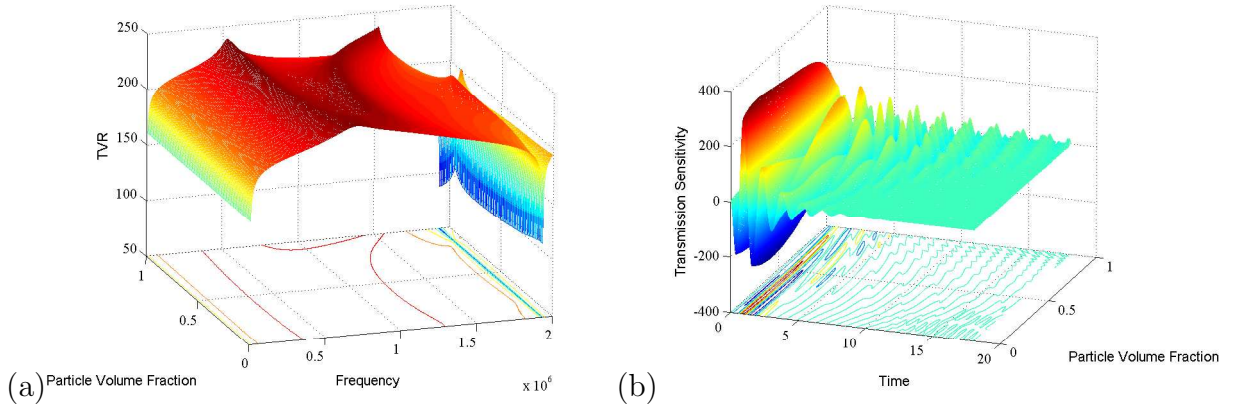

Figure 7: (a) The Transmission Voltage Response (TVR (dB)) against frequency (Hz) and (b) the transmission sensitivity (N/V) against time (μs), versus the volume fraction of particles in the matching layer (φ).

metrics which describe the efficiency of the device. In Figure 5(a) the 3dB bandwidth of the TVR is shown as a function of the particle volume fraction, when the magnetic field is absent (i.e. $H = 0$ and so $\bar{\varphi} = \varphi$). As anticipated from the preceding discussion, the maximum bandwidth corresponds to a particle volume fraction of roughly $\varphi = 0.3$. However there is a discontinuity in the profile at this point and later at $\varphi = 0.55$ that

17

can be explained by examining Figure 7(a). As can be seen the TVR is unimodal for low volume fractions but as the volume fraction is increased two peaks appear that gradually separate and sharpen. In addition, the location of the maximum peak switches from the lower frequency peak to the higher frequency peak (see Figure 6(a)). As the valley lying between the two peaks deepens, the frequency of the left hand limit of the bandwidth (f_l) abruptly jumps from outside this valley (at a lower frequency) to inside this valley. This then leads to a jump discontinuity in the bandwidth calculation given by equation (15). As the amplitude (gain) of both peaks is similar the gain bandwidth product mirrors the jump seen in the bandwidth profile (see Figure 5(b)). As φ increases the mechanical impedance of the matching layer increases beyond the optimal value and this leads to reduced efficiency in transmitting the mechanical energy of the device to the load medium. This internal energy manifests itself as an additional mode of vibration in the system characterised by the two peaks in Figure 7(a). As this problem becomes more acute at higher volume fractions the piezoelectric layer and the matching layer almost decouple with the higher frequency mode corresponding to the thin and stiff matching layer. The lower frequency mode is approximately equal to the electrical resonant frequency of the piezoelectric layer in vacuum ($f_e = 723$ KHz). In Figure 6(b) the ringdown time, as defined by equation (14), is shown as a function of the particle volume fraction. This has a minimum value of $R = 3.9\mu$s at around $\phi = 0.1$. This volume fraction is considerably lower than that found for the optimum bandwidth but, as can be seen in Figure 7(a), at $\varphi = 0.3$ the TVR profile is bimodal with some steep slopes. At lower volume fractions a unimodal response is seen with shallow slopes corresponding to a reduced ringdown time. This dependency of the ringdown time on φ is shown in Figure 7(b).

The final set of figures show the dependency of the device's efficiency on the magnetic field strength. In Figure 8(a) the bandwidth is plotted as a function of H at a volume fraction of $\varphi = 0.5$. A single maximum is found at around $H = 70$ Gauss; slightly higher
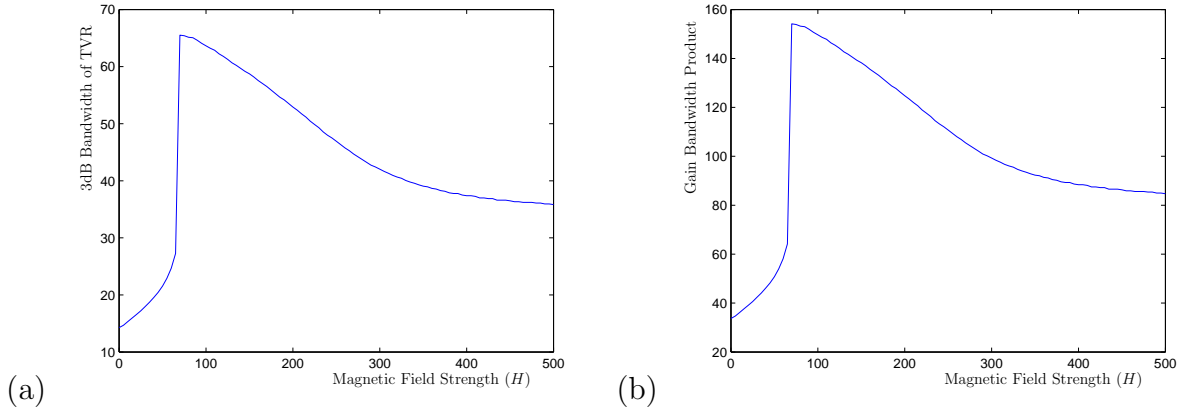
Figure 8: (a) The 3dB bandwidth of the Transmission Voltage Response (TVR) and (b) the Gain Bandwidth Product versus the magnetic field strength in the matching layer (H (Gauss)).
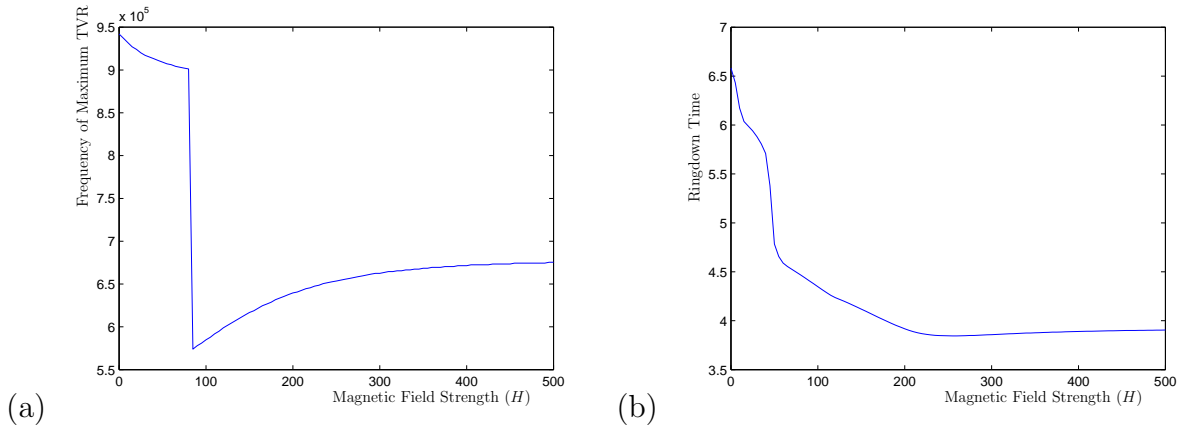
Figure 9: (a) The frequency (Hz) of the peak Transmission Voltage Response and (b) the ringdown time (μs), versus the magnetic field strength in the matching layer (H (Gauss)).

than the previous optimum value discussed in relation to Figure 3(a). However, if the bandwidth calculation was performed for only the lower frequency peak (see Figure 9(a)) then the upper branch in Figure 8(a) would extend into the lower volume fractions and may indeed have its maximum at a lower value of H. This agrees with Figure 10(a) where the gradient near the peaks and the separation of the peaks is less pronounced than that in
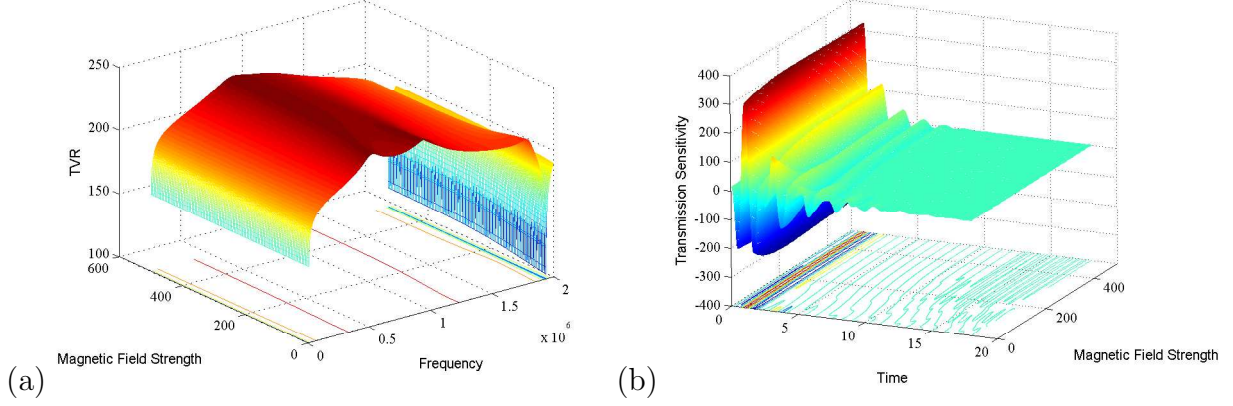
19

Figure 10: (a) The Transmission Voltage Response (TVR (dB)) against frequency (Hz) and (b) the transmission sensitivity (N/V) against time (μs), versus the magnetic field strength in the matching layer (H (Gauss)).

Figure 7(a). Again the GBP follows the bandwidth profile in Figure 8(b). In Figure 9(b) the ringdown time is plotted as a function of H. At $H = 0$ the ringdown time of 6.5 μs corresponds to the ringdown time shown in Figure 6(b) at $\varphi = 0.5$. As H increases the effective volume fraction $\bar{\varphi}$ decreases and so the monotonically decreasing curve shown in Figure 9(b) corresponds to a traversal of Figure 6(b) in the direction of decreasing volume fraction starting from $\varphi = 0.5$. As H increases the effective volume fraction attains its limiting value of $\varphi_{sat} = 0.052$ and so the upward turn, seen at very low particle volume fractions (i.e. less than 0.052) in Figure 6(b), is not seen in Figure 9(b). The ringdown time does achieve a minimum value (a very shallow minimum) of around 3.8 μs at around $H = 230$ Gauss. In Figure 10(a) the TVR changes from a bimodal response to a unimodal response as the magnetic field is increased. This unimodal distribution slightly sharpens for very high magnetic field values and hence the optimum time domain response occurs at an intermediate value. The time domain plot in Figure 10(b) illustrates this further.

Having investigated the behaviour of the device as a function of two of the design parameters (volume fraction of iron particles in the matching layer and the magnetic field

20

	$H = 0$		
Z_L	Ringdown	3dB BW	GBP
1.5 MRayls	4.55 μs	27.3	64.2
1.0 MRayls	6.66 μs	14.2	33.4

	$H = 500$		
Z_L	Ringdown	3dB BW	GBP
1.0 MRayls	4.9 μs	27.2	64.1

Table 7: Enhanced ringdown time, 3dB bandwidth and gain bandwidth product (GBP) using the active matching layer ($\varphi = 0.3$).

strength) it is useful to then examine how a given device could react to external influences to enhance the device's performance. The active layer provides an additional degree of freedom that allows the transducer to be finely tuned once deployed. This could help in instances where the external environment is changing. For example, the mechanical load could vary from one patient to another depending on the region of the body being investigated, or the salinity or depth of water could affect the mechanical load in sonar applications. In Table 7 one such scenario is explored. When the mechanical load Z_L^s is decreased from 1.5 MRayls to 1.0 MRayls there is a marked increase in the ringdown time and a corresponding decrease in the bandwidth. By switching the magnetic field on ($H = 500$ Gauss) in the active matching layer the device adjusts for this external change and recovers the original efficient performance.

5 Conclusions

A piezoelectric transducer comprising of an active piezoelectric layer sandwiched between a backing material and an active matching layer has been theoretically modelled and analysed. It was found that the additional flexibility of an active matching layer can be used to maintain the efficiency of the device as external loads vary. The active layer provides an additional degree of freedom which allows the transducer to be finely tuned once deployed. The mechanical load was varied in the model and this resulted in a marked increase in the ringdown time and corresponding decrease in the bandwidth. By switching the magnetic field on in the active matching layer it was found that the device adjusted to this external change and recovered the original efficient performance. This transducer concept could also useful when investigating fluid-solid phase transitions and other physico-chemical reactions.

References

[1] G. Hayward, "The influence of pulser parameters on the transmission response of piezo-electric transducers.", *Ultrasonics*, Vol. 23, No. 3, pp. 103-112, (1985).

[2] Y. Nahmad-Molinari, C.A. Arancibia-Bulnes, and J.C. Ruiz-Suarez, "Sound in a Mag-netorheological Slurry.", *Phys. Rev. Letts.*, Vol. 82, No. 4, pp. 727-730, (1999).

[3] G. Hayward, "A systems feedback representation of piezoelectric transducer operational impedance.", *Ultrasonics*, Vol. 22, No. 4, pp. 153-162, (1984).

[4] G. Hayward, C.J. MacLeod and T.S. Durrani, "A Systems Model of the Thickness Mode Piezoelectric Transducer.", *JASA*, Vol. 76, No.2, pp. 369-382, (1984).

[5] G. Hayward, "Using a block diagram approach for the evaluation of electrical loading effects on piezoelectric reception.", *Ultrasonics*, Vol. 24, No. 3, pp. 156-164, (1986).

[6] G. Hayward and J.A. Hossack, "Unidimensional Modelling of 1-3 Composite Transducers.", *JASA*, Vol. 88, No. 2, pp. 599-607, (1990).

[7] W.A. Smith and B.A. Auld, "Modelling 1-3 Composite Piezoelectrics: Thickness-Mode Oscillations.", *IEEE Trans UFFC*, Vol. 38, No. 1, pp. 40-47, (1991).

[8] D.A. Berlincourt, D.R. Curran and H. Jaffe in: *Physical Acoustics Principles and Methods.* Vol. 1(A), W.P. Mason (Ed.), Academic Press, New York (1964).

[9] A.H. Harker and J.A.G. Temple, "Velocity and Attenuation of Ultrasound in Suspensions of Particles in Fluids.", *J. Phys. D: Appl. Phys.*, Vol. 21, pp. 1576-1588, (1988).

[10] R.T. Beyer and S.V. Letcher, *Physical Ultrasonics*, Academic Press, London, (1969).

[11] R.L. O'Leary, G. Smillie, G. Hayward and A.C.S. Parr, *CUE Materials Database*, Technical Report, Centre for Ultrasonic Engineering, University of Strathclyde, Glasgow, Scotland, (2002), *www.cue.ac.uk*.

[12] Ferroperm UK Ltd, Vauxhall Industrial Estate, Ruabon, Wrexham, United Kingdom, LL14 6HA.

[13] Huntsman Advanced Materials Ltd, Ickleton Road, Duxford, Cambridge, United Kingdom, CB2 4QA, *www.huntsman.com*.